Original scientific paper

Tracking the photoactivity at the interface of SiC/poly(2-(2--thienyl)furan) thin solid film in polymer gel electrolytes

Kasem K. Kasem[✉], Hisako Masuda and Andrea Mendez Rodriguez

School of Science, Indiana University Kokomo, Kokomo, IN, 46904, USA

Corresponding authors: [✉] *kkasem@iu.edu; Tel. 765-455-9245*

Abstract

Assemblies made by immobilizing silicon carbide (SiC) nanoparticles into poly(2-(2-thienyl)furan) (PTF) were subjected to optical and electrochemical investigation. The studies show that SiC, a molecular inorganic compound, and PTF produce reproducible photo responses. Optical studies show that the optical band gap of SiC is around 2.5 eV while PTF's is around 2.2 eV. The band gap values suggest these assemblies absorb the visible solar radiation spectra. Electrochemical studies in gel electrolytes indicate that PTF and PTF/SiC under illumination show p-p behavior, where hole accumulation dominates. SiC thin films lack such character. Electrochemical impedance spectroscopy studies revealed that the PTF and PTF/SiC possess both kinetic and diffusional charge transfer properties. The studied assemblies, as well as the gel electrolyte, showed stability and resistance to photodegradation as evidenced by the regeneration of the same photo response after a longer period of experimentation.

Keywords

Photoelectrochemistry, occlusion electrodeposition, polymer/molecular solid interfaces, theoretical-experimental approach, polymer electrolyte

Introduction

Monomer-based heterocyclic building blocks containing different heteroatoms have generated photoactive organic-polymer semiconductors (OSC). Heterocycle monomers with sulfur or nitrogen possess a flat π-conjugated network that offers several benefits over their benzene-based compound. Some of these benefits are: 1) resistance for air oxidation that is achieved *via* lowering the highest occupied molecular orbital (HOMO) due to the higher electronegativities of S and N, 2) the structural manipulation is easier through S…N centers, and 3) the S-larger π-orbitals that allow stronger orbital overlap and consequently lead to enhanced electronic communication between molecules [1-6]. These polymers have applications in organic light-emitting diodes [7], field-effect transistors [8], electrochromic windows [9], sensors [10], and solar cells [11]. While most commercially produced organic conductors are prepared by chemical polymerization [12], many

monomers can be electropolymerized directly on a metal or semiconductor electrode [13,14]. Electropolymerization allows in situ electrochemical and spectroscopic studies of the polymer.

Oxygen (the heteroatom in the furan ring) has a considerably smaller covalent radius than sulfur, which could reduce the distance of p-p stacking for the charge carrier transfer. Sulfur has a relatively lower electronegativity at 2.5 and a larger covalent radius. This creates a larger p-p stacking than in oxygen. In both furan and thiophene, the dipoles are directed toward the heteroatoms. At the same time, the furan has a dipole moment of 0.71D, which is larger than the thiophene ring of 0.54D [15]. The building blocks with different heteroatoms (fused or unfused) generate various dipole moments in the structures and ultimately can make tuning the HOMO/LUMO levels and band gaps [16]. However, due to the difficulty of molecular structure modification, weak light absorption, and low efficiency of fused ring donors or acceptors [17,18], attention turns to polymer-based unfused heterocyclic monomers with different heteroatoms.

Creating heterojunctions consisting of organic/inorganic semiconductor interfaces (O/I/I) to get enhanced photoactive assemblies has been explored [19-22]. The inorganic components of these assemblies were metal oxides or chalcogenides. A little has been done using molecular-covalent solid compounds such as silicon carbide (SiC) as an alternative for metal oxides or chalcogenides in these O/I/I assemblies. SiC powder has several applications in semiconductor technology and photovoltaic energy [23]. This is due to its enhanced material properties and moderate band gap, which allow the absorption of short-wave visible solar radiation. Previous studies [24] investigated assemblies made of graphene and SiC as an O/I/I heterojunction.

In the present work, we studied the photoactivity of SiC/poly(2-(2-thienyl)furan) (PTF) assemblies created by the occlusion electrodeposition method. The prepared assemblies were subjected to optical and photoelectrochemical (PEC) studies in a gel electrolyte. The objectives of this study are to investigate the effect of furan π-bridge on the photo-activities of the interface and further the mutual influence of PTF and SiC on the PEC behavior of each other in polymer gel electrolytes.

Experimental

All materials used were of analytical grade. 2-(2-thienyl)furan (TF) was used as received.

Instrumentation

All electrochemical experiments were carried out using either a conventional three-electrode cell or an electrochemical cell previously described [25]. A BAS 100W electrochemical analyzer (Bioanalytical Co.) was used to perform the electrochemical studies, such as cyclic voltammetry (CV) and chronoamperometry (CA). Steady-state reflectance spectra were performed using Shimadzu UV-2101 PC. Irradiations were performed with a solar simulator 300-watt xenon lamp with an IR filter (Newport). Electrochemical Impedance spectroscopy was carried out using a Solartron 2101A. Photoelectrochemical studies of the thin solid films in gel electrolyte were performed using $2.0\ cm^2$ fluorine-doped tin oxide (FTO) covered with the photoactive material as a working electrode, and platinized FTO (Pt-FTO) served as both reference and counter electrode. Unless otherwise stated, all potentials were measured against platinized FTO (0.597 V *vs*. SHE).

Occlusion electrodeposition of SiC/PTF

A CV technique was used to occlude SiC nanoparticles into PTF. In a typical 3-electrodes cell, FTO is the working electrode, Ag/AgCl is the reference electrode, and Pt sheet is the counter electrode. A compact thin film is formed by repetitive cycling (3 cycles) of the FTO glass electrode potential in

a suspension of SiC (1 mg/mL) in acetonitrile solution containing 5 mM of TF monomer and 0.2 M LiClO$_4$ between -0.5 V and 1.7 V *vs*. Ag/AgCl.

Preparation of gel electrolyte

Polymer gel electrolyte was prepared as previously described [26]. Briefly, 0.065 M KI and 0.065 M I$_2$ (to form I$^-$/I$^-_3$) were dissolved in 10 mL propylene carbonate (PC), and then 8.5 g of polyethylene glycol (PEG M-8000) was added to the mixture. The mixture was heated at 100 °C under continuous stirring for *ca.* 12 h in a flask under an inert atmosphere, the mixture was further heated at 180 °C for 14 h hydrothermal treatment in a Teflon autoclave.

Computational procedures

To provide further mechanistic insights into the observed trend in PTF's photoactivity, we carried out quantum mechanical calculations using Orca version 5.0.4 [27]. The geometries were optimized by the density functional theory (DFT) method B3LYP with the def2-TZVP basis set. The energy of the highest occupied molecular orbital (HOMO) and the lowest unoccupied molecular orbital (LUMO), as well as energy gaps, were calculated for the optimized structures using B3LYP + D3/def2-SVP level of theory. The orbitals were visualized using IboView [28]. Our work was performed using Indiana University's high-throughput computing cluster, Quartz.

Results and discussion

Electropolymerization of 2-(2-thienyl)furan

Thin films of PTF on FTO were prepared using an oxidative electropolymerization method by repetitively cycling the potential of FTO (as substrate) at a scan rate of 0.1 V/s between -0.50 and 1.5 V *vs*. Ag/AgCl in acetonitrile solution containing 5 mM of the monomer TF, and 0.2 M LiClO$_4$. The results are displayed in Figure 1.
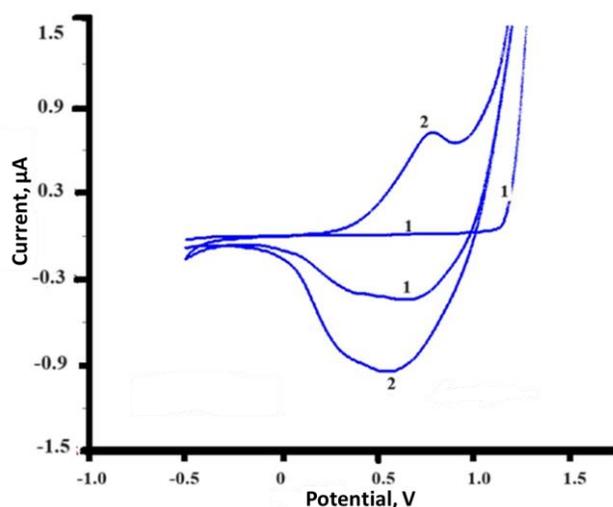
Figure 1. *Oxidative electropolymerization on FTO from 5 mM 2-(2-thienyl)furan (TF) in 0.2 M LiClO$_4$ in acetonitrile at a scan rate of 0.1 V/s. Scan numbers are shown in the figure*

This figure shows that the first oxidative electropolymerization on the FTO surface (the first scan) occurred at ≈1.2 V *vs*. Ag/AgCl. The second scan indicates that the oxidation process took place at ≈1.0 V. The second scan represents monomer oxidation on partially or fully covered FTO with PTF. It is worth noting that a growth of cathodic peak in a potential range of 1.0 to 0.2 V *vs*. Ag/AgCl upon repeating the scans. These cathodic peaks will appear only if the anodic scan reaches 1.2 V. Because multiple products are produced from the oxidation process, definitive values of oxidation and

reduction potentials cannot be determined. This resulted in an uncertain value for the electrochemical band gap. Therefore, our study utilized the optical bandgap to interpret some observations. Absorption spectra of the polymer/oligomer films on the electrode are more reliable sources of experimental data that can be compared with computational studies.

Optical/spectroscopic studies

Optical parameters, such as absorbance and conductivity, σ_{opt}, have been calculated and plotted as a function of photon energy. Theoretical values for the band gas were calculated by the DFT method. The results are displayed in Figures 2-6.

Optical band gap studies

Figure 2A shows the absorption spectra of the PTF, where absorption is plotted against the photon energy of incident light. Figures 2B and C were prepared after treatment of the absorption data as plots of $\alpha^{1/2}$ *vs.* photon energy (*hv*) and $(\alpha*hv)^2$ *vs.* hv respectively, as described in previous studies [29]. Figure 2A shows an approximate optical band gap at 2.4 for PTF, and the assembly shows greater absorption in the range of photon energies between 2.0 and 2.8 eV. However, the maximum absorption took place at λ = 445 nm. The value of the band gap corresponding to this wavelength is 2.8 eV. Figure 2C indicates the existence of a direct band gap of 2.4 eV. Comparing this experimentally determined value of 2.4 eV as a band gap with the calculated DFT data listed in Table 1, plotted in Figure 3 suggests that it corresponds to at least septum units of bi-heterocyclic TF monomers connected to form cyclic oligomers as shown in Figure 4.
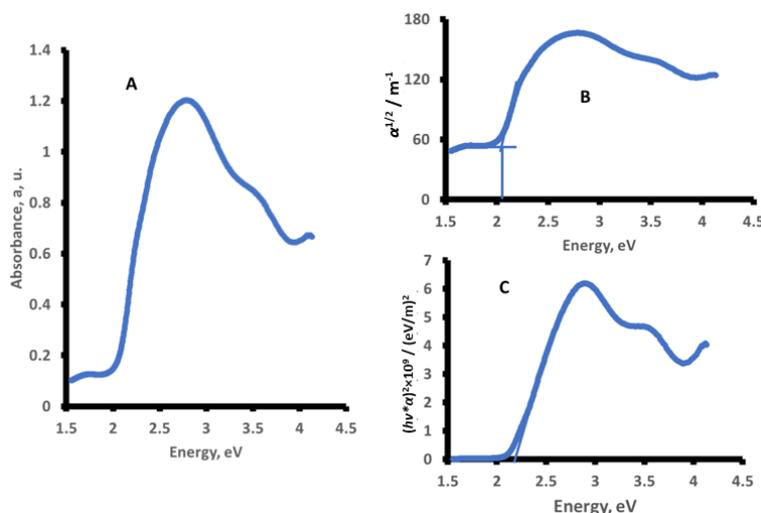
Figure 2. *Absorption spectra for PTF film: A) Absorbance* vs. *photon energy,*
B) $\alpha^{1/2}$ vs. photon energy, and C) $(\alpha* hv)^2$ vs. photon energy

Computational studies

DFT calculations were performed with the B3LYP/def2-TZVP model and the energy difference (gaps) between the (HOMO and LUMO were calculated for the optimized structures and listed in Table 1.

The global reactivity parameters were calculated from the HOMO-LUMO *energies* after Koopmans' theorem [30]. The HOMO reveals the electron donor capability = (oxidation) ionization potential (IP), whereas the LUMO describes the capacity to accept an electron = (reduction) electron affinity (EA). Equations used to calculate hardness (η), electronegativity (χ), softness (Š), electrophilicity (ϵ), and the fraction of electrons transfer between the assemblies and the FTO interface (ΔN) are described in the previous work [31].

Table 1. Calculated band gap and other characters for possible oligomers of TF using DFT

Number of units	$1/n$	E_g / eV	χ
1	1.0	4.28	3.42
2	0.50	3.11	3.45
3	0.33	2.70	3.47
4	0.25	2.51	3.49
5	0.20	2.40	3.59
6	0.16	2.23	3.47
8	0.125	2.20	3.47

Table 1 shows that the HOMO-LUMO energy gap of oligomer with >6 monomer units is closer to what was found experimentally at ≈2.3 eV (Figure 2). This also suggests that the assemblies with such cyclic oligomers follow a direct band gap (Figure 2 C). The calculated EA of PTF is smaller than that of 2.6 eV listed for PTF in Table 2. The limits of the assumption with IP ≈ band gap + EA may explain such values. Table 2 summarizes the reactivities of PThF on FTO such as η, χ, $\check{S}$, ϵ and ΔN. This increase of ΔN for SiC is evidence of increasing electron transfer between the SiC/FTO than on the PFT/FTO interface. Furthermore, the hard/soft acid-base characteristics (HSAB) and the greater electrophilicity (ϵ) of PTF than that of SiC indicate the *p*-type nature of PTF and stronger adsorption on the FTO surface than SiC. This adsorption facilitates the electron transfer at the electrolyte/elec-trode interface.

Table 2. The optical band gap and other acid/base characters for the studied compounds

Assembly	χ	Direct band gap, eV	EA, eV[a]	IP, eV	η / Pa	$\check{S}$ / Pa^{-1}	ϵ / Pa^{-1}	ΔN
SiC	2.2	2.6	3.8	6.4	1.3	0.77	1.86	0.21
PTF	3.40	2.2	2.6	4.8	0.55	1.8	10.51	0.007
FTO	3.35	3.45	1.65	5.1	1.73	0.578	0.865	

[a]assuming that IP ≈ band gap + EA
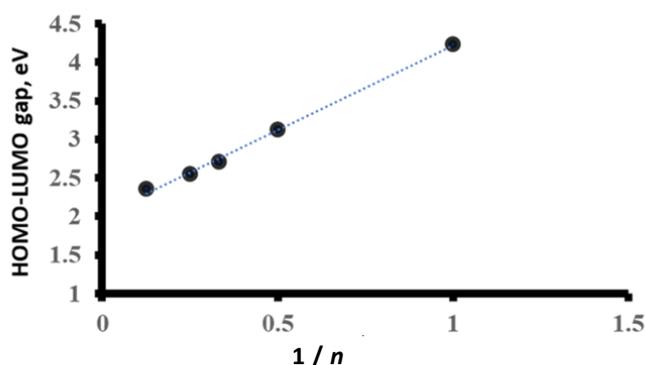
Figure 3. HOMO-LUMO gaps vs. number of TF monomers based on DFT calculation
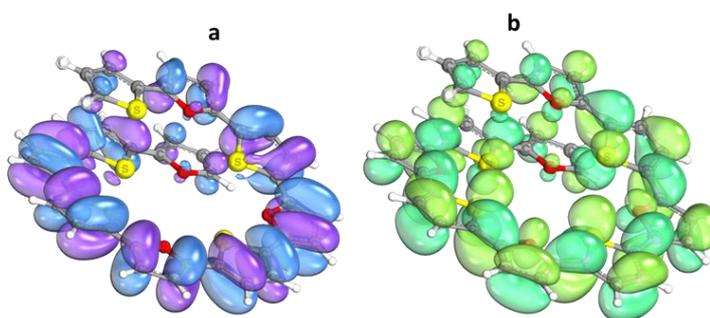
Figure 4. a) LUMO and b) HOMO orbitals of the cyclic oligomer (7 units of TF), calculated using DFT

Figure 5 shows the absorption spectra for SiC thin film. Figure 5A shows multiple absorption peaks between 2.3 to 3.55 eV. Such results suggest that the SiC sample can be a mix of 3C-SiC, 6H-SiC, 4H-SiC, and 2H-SiC. While 3C-SiC has a band gap of 2.2 eV 6H-SiC, 4H-SiC, and 2H-SiC possess 3.0 eV, 3.3 eV, and 3.5 eV, respectively [32,33]. The band gap increases with increasing its hexagonal character. Figures 5B and 5C indicate the possible existence of direct and indirect band gaps in this amorphous structure. Figure 6 shows that the occlusion of SiC into PTF increases the absorption of light radiations corresponding to photon energies between 1.7 to 2.2 eV (Figure 6 trace 1). The occlusion of SiC in PTF may create hybrid sub-bands with smaller band gaps between HOMO and LUMO of the host polymer. This explains the absorption of longer wavelengths of radiation.
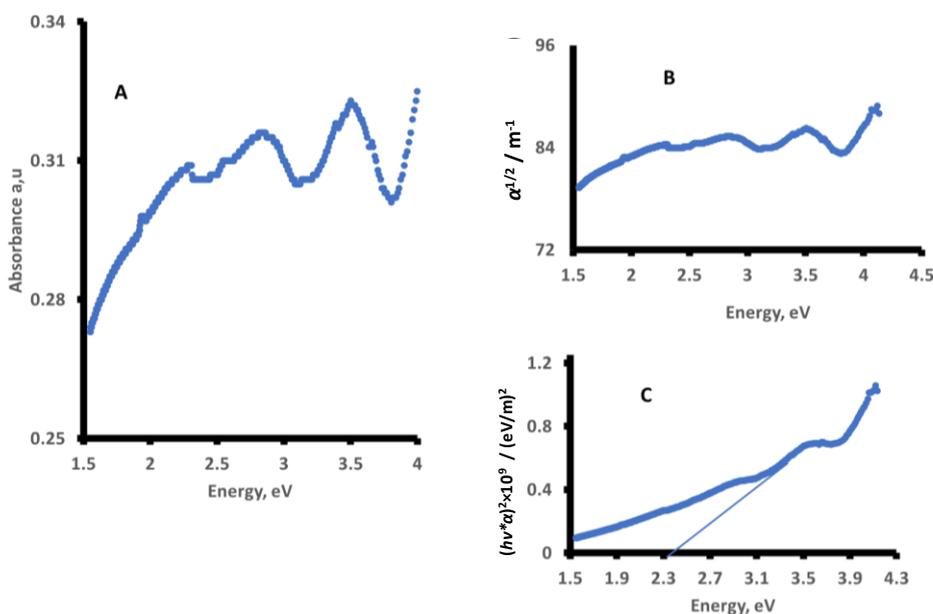
Figure 5. *Absorption spectra for SiC film: A) Absorbance* vs. *photon energy, B)* $\alpha^{1/2}$ vs. *photon energy, and C) (α*hν)^2* vs. *photon energy*
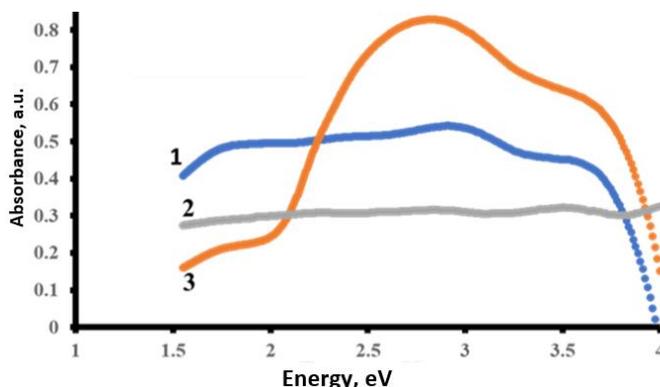
Figure 6. *Absorption vs. photon energy for a thin film of: 1) SiC/PTF, 2) SiC, and 3) PTF*

Optical conductivity

Optical conductivity (σ_{opt}) and electrical conductivity (σ_{ele}) were calculated using equations (1) and (2) [34,35]:

$$\sigma_{opt} = \alpha nc/4\Pi \tag{1}$$

$$\sigma_{ele} = 2\lambda\sigma_{opt}/\alpha \tag{2}$$

where α is the absorption coefficient, n is the refractive index, c is the velocity of light, and λ is the wavelength. The plots of σ_{opt} and σ_{ele} *vs.* photon energy for PTF, SiC, and SiC/PTF are displayed in Figure 7. Figures 7 A and B show that σ_{opt} for PTF is greater than that of SiC/PTF or SiC within the

studied photon energy. It reaches the maximum value around the band gap of each assembly. Optical conductivity is related to the light–electrical component and it is time-dependent. The electrical component of light varies its amplitude and direction over time [36]. The lower optical conductivity of SC/PTF than that of PTF at all photon energy can be explained on the basis that the presence of the molecular SiC hinders the interaction of the polymer with the electric component of light. However, Figure 7C shows that the electrical component of the optical conductivity decreases as the photon energy increases. This may be attributed to the increase of the activity caused by electron collisions with thermal photons. Such an increase in this electron collision may reduce the "mean free path" of electrons, increasing the resistivity of the conductor.
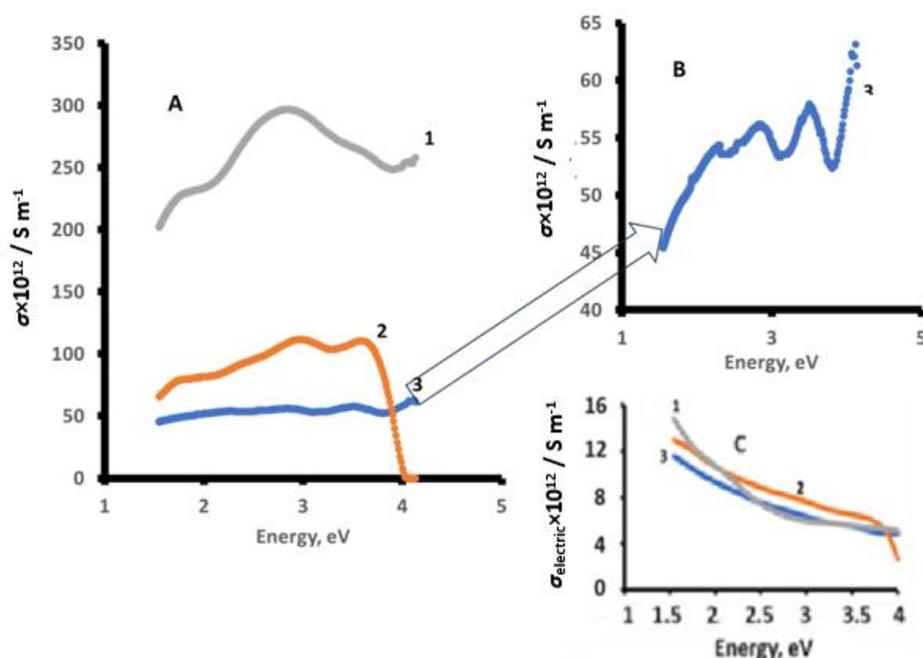
Figure 7. A) Optical conductivities of 1) PTF, 2) PTF/SiC, and 3) SiC. B) Exploded view for track 3 in A), and C) calculated σ_{ele} vs. photon energy

Photoelectrochemical (PEC) studies

Electrochemical behavior of PTF thin film

Unless otherwise stated, PEC studies were performed in the dark and under illumination with a scan rate of 0.10 V/s between -1.5 to 1.0 V. The results are displayed in Figure 8A. It can be noticed that upon illumination, there is an increase in the photocurrent for PTF/FTO in both anodic and cathodic scans. However, more photocurrent was reported in the cathodic scan. Figure 8A also shows that a noticeable photocurrent was first reported at ≈0.8 V *vs.* platinized FTO (0.597 V *vs.* SHE). This indicates an approximate position of the Fermi level at 5.0 eV.

Figure 8B shows a sudden increase in photocurrent upon illumination. This indicates the presence of hole accumulation at the interface FTO/PTF. Such behavior is expected for the p-type nature of organic semiconductor polymers. When a p-p type heterojunction is created, possible hole accumulation can take place. The amount of hole accumulations and the transient current time constant can be quantitatively calculated. The concentration of accumulated holes was calculated by integrating the area under each spike considering the charge density and photochemical equivalence law. Figure 8B also shows a steady decrease in the amount of hole accumulation in the consecutive trials. Furthermore, the transient time constant for the accumulated charges was calculated using the following equation [37].
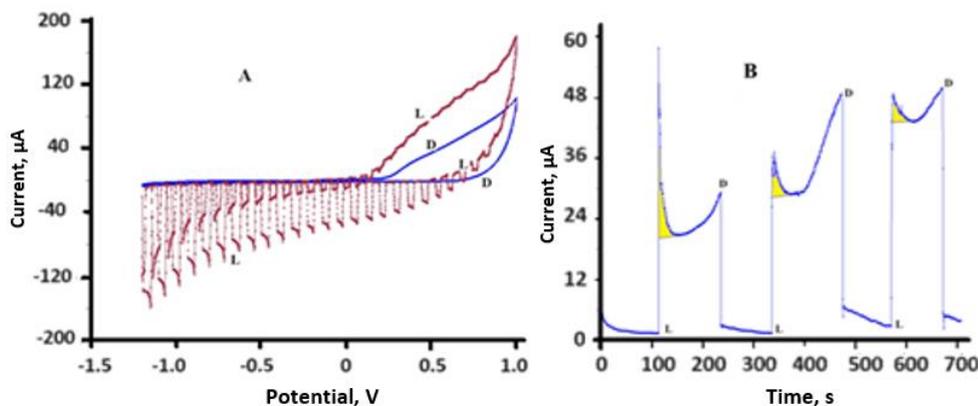
Figure 8. *A) I vs E at scan rate 0.1 V s⁻¹ for PTF/FTO/gel electrolyte, and B) chronoamperometric studies at -1.0 vs. platinized FTO for PTF/FTO. (D =dark, L =under illumination)*

$$R = e^{-\frac{t}{\tau}} \qquad\qquad (3)$$

where t is time, τ is the transient time constant, and $R = (I_t - I_{st})/(I_{in} - I_{st})$, as I_t is current at time t, I_{in} is immediate photocurrent, and I_{st} is the stationary value of photocurrent (steady current). The plot of ln R *vs.* time (Figure 9) generates a straight line with slope = $1/\tau$. The reciprocal of the slope determines the value of τ in seconds. The calculated τ is ≈7 seconds.

$$y = -0.1397x + 0.0448$$
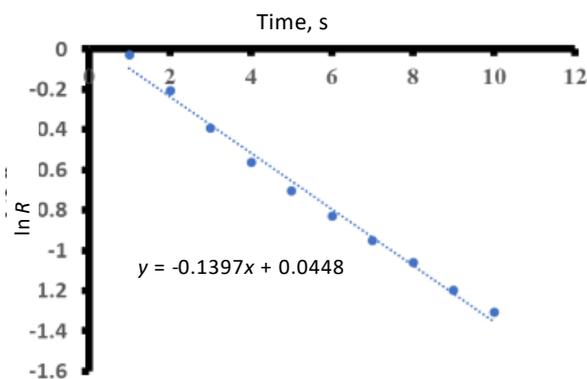
Figure 9. *ln* R vs. *time for data displayed in Figure 8B*

Effect of occluded SiC in PTF

FTO modified by PTF occluded with SiC was subjected to CV studies in the dark and under illumination. The results are shown in Figure 10A.
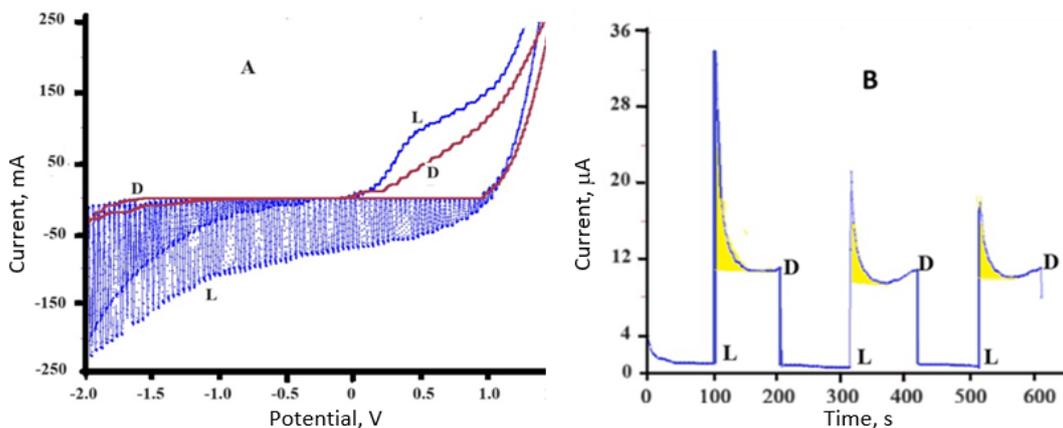
Figure 10. *A) I vs. E at scan rate 0.1 V/s for SiC/PTF/FTO/gel electrolyte, B) chronoamperometric studies at -1.0 V vs. platinized FTO for SiC/PTF/FTO. (D =dark, L =under illumination)*

As observed previously with PTF/FTO, upon illumination, there is an increase in the photocurrent for SiC/PTF/FTO in both anodic and cathodic scans. However, more photocurrent was reported in the cathodic scan. The generated photocurrent from SiC/PTF/FTO film is greater than that of PTF/FTO. Figure 10B displays a pattern like that observed in Figure 8B, which shows a reproducible sudden increase in photocurrent upon illumination. This indicates that the occlusion of SiC into PThF maintains the process of hole accumulation at the interface. The calculated transient time constant was ≈7 seconds.

Electrochemical behavior of SiC thin film

Suspensions of amorphous SiC in acetonitrile/LiClO4 were evenly spread over the FTO surface. The electrochemical behavior of SiC/FTO in gel electrolyte studies was performed in the dark and under illumination, with a scan rate of 0.10 V/s between -1.5 and 1.0 V. The results are displayed in Figure 11A. The illuminated interfaces generated photocurrent in both cathodic and anodic scans. Photocurrent starts exceeding the recorded dark current at ≈0.5 V *vs.* platinized FTO. This indicates an approximate position of the fermi level at 4.3 eV. The occlusion of SiC has added more photo activities to PTF, as is evident from the higher photocurrent at -1.0 V (Figure 11A).
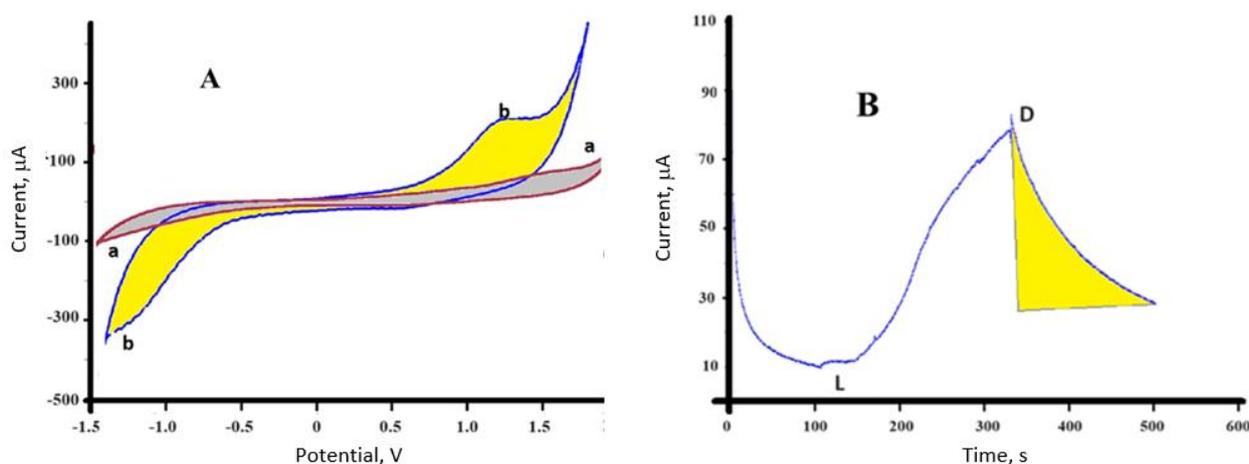
Figure 11. *A) I vs. E at scan rate 0.1 V/s for SiC /FTO/gel electrolyte, a) dark, b) illumination, and B) chronoamperometric studies at -1.0 V vs. platinized FTO for SiC/FTO. (D =dark, L =under illumination)*

Figure 11B displays the chronoamperometric studies at -1.0 V for SiC/FTO. This figure shows a gradual increase in photocurrent and the lack of a sudden rise in photocurrent. This indicates that the studied FTO/SiC interfaces did not generate hole accumulation. This figure also shows no sudden drop in the measured current under-dark conditions. Instead, a gradual drop of the measured current took place for ≈250 s (shaded area). The current generated in the absence of incident light photons is known as dark current, which may reflect the random generation of electrons and holes within the depletion region at the FTO/SiC interface [38,39]. This can be attributed to the amorphous nature of SiC.

Electrochemical impedance spectroscopy

EIS of the studied assemblies FTO/SiC, FTO/PTF, and FTO/PThF/SiC in gel electrolyte were achieved between 10^5 and 10^{-1} Hz. Nyquist plots, as well as other dielectric properties generated from the assemblies on FTO substrate in the dark and under illumination, are displayed in Figures 12 and 13. Figure 12 shows kinetic but larger diffusional control across the studied frequency range. Impedance studies indicate film porosity as evident from the shape of the Nyquist plot at high frequencies and Warburg impedance at low frequencies [40].
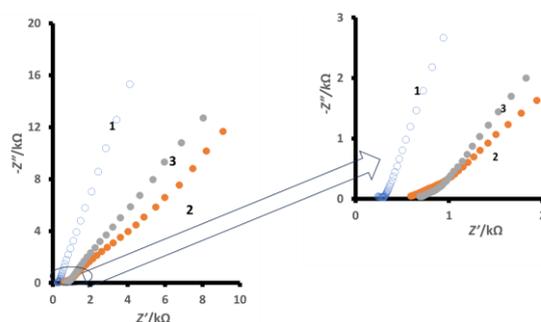
Figure 12. *Nyquist plot at 0.0 V vs. platinized FTO for Illuminated: 1) FTO/SiC, 2) FTO/PTF, and 3) FTO/PTF/SiC*

The redox capacitance C_L(Farad) can be calculated from the slope of (-Z'' *vs.* $1/\omega$) plot (not shown). Analysis of the plot at the very low frequencies portion of the Warburg section shows the following quantities, 65.7, 59.0 and 42.2 µF for FTO/SiC, FTO/PTF, and FTO/PTF/SiC, respectively.

Figure 13 shows the Nyquist plots at 0.0 V *vs.* platinized FTO for A) FTO/PTF, B) FTO/SiC/PTF, and C) FTO/SiC. Figure 13A demonstrates that illumination of the host polymer (PTF) decreases the imaginary component of impedances at all applied frequencies. However, Figure 13B indicates that hosting SiC shows such a decrease at low frequencies. Figure 13C shows no changes occur upon illumination of the assembly FTO/SiC. Such behavior may be due to the formation of different phases caused by the occlusion of SiC in PTF. Figure 13 further shows that the studied assemblies showed a behavior of a porous film structure that never reached a status of charge saturation at very low frequencies. The different portions of the Nyquist plot show the Warburg zone.
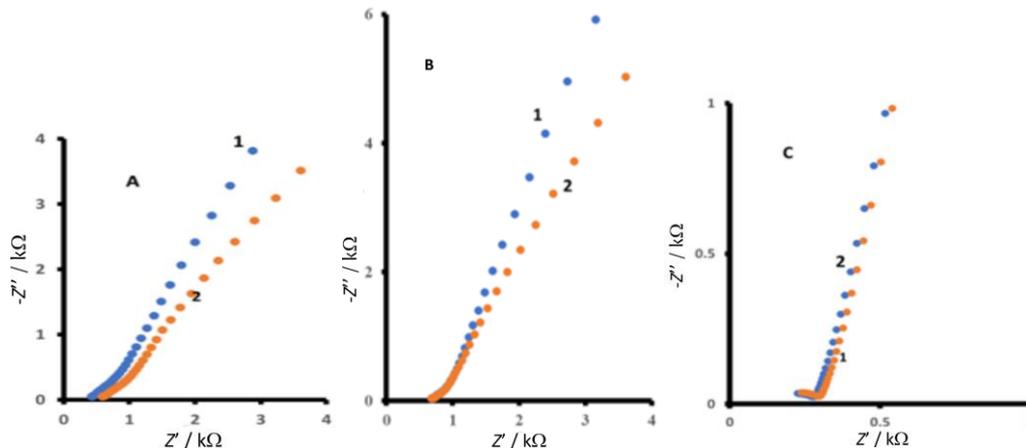
Figure 13. *Nyquist plot at 0.0 V vs. platinized FTO for A) FTO/PTF, B) FTO/SiC/PTF, and C) FTO/SiC (1 = dark, 2 = under illumination)*

Figure 14 plots log σ (conductivity) *vs.* log ω (frequency). Under illumination, the AC conductivity of FTO/SiC/PTF (Figure 14A) and of FTO/PTF (Figure 14B) increases by raising the frequency for studied assemblies to ≈100 Hz, after which the conductivity becomes independent of frequency for FTO/SiC/PTF. However, illumination decreases the AC conductivity for FTO/PTF, especially at frequencies greater than 100 Hz. It is worth mentioning that the conductivity of FTO/SiC was similar but not identical to that displayed in Figure 14A. Illumination did not cause any changes in AC conductivities at frequencies greater than 1KHz. This behavior was observed and explained on the basis that at high frequencies, the increased capacitive reactance of the studied assembly is a major factor in the observed conductivity decrease [41].
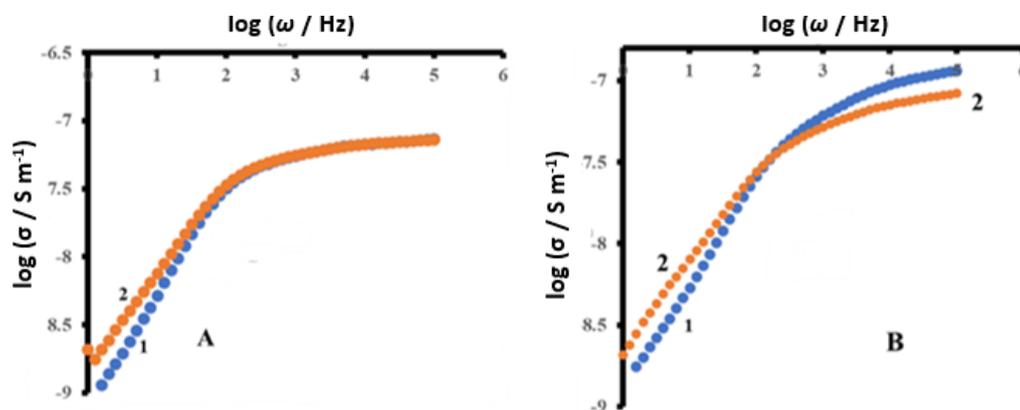
Figure 14. *Log electrical conductivity (σ) vs. log frequency (ω) of the A) FTO/SiC/PTF, and B) FTO/PTF (1 = dark, 2 = under illumination)*

Conclusion

Photoelectrochemical behavior of SiC particles occluded in PTF in polyethylene glycol-based gel electrolyte shows that the molecular SiC solid particles have integrated photo activities within the PTF as a host photoactive polymer. Chronoamperometric studies suggest hole accumulation upon illumination of FTO/PTF and FTO/SiC/PTF interfaces. On the other hand, the illuminated FTO/SiC interface lacks such a phenomenon but shows dark current phenomena. This reflects a case of random electron and hole generation at the FTO/SiC interface. EIS shows evidence for small kinetically controlled and major diffusional controlled charge transfer. The diffusion portion reflects that all studied assemblies are porous amorphous structures. Results show that the photoactivity outcome of SiC and PTF was due to mutual interactions between molecular solid SiC and the conductive photoactive PTF and the 2(2-thienyl) furan π-bridge did not alter the photo-activities of the interface. The data in Table 2 reflects an energy map for staggered band gap alignment between SiC and PTF. Such alignments offer better charge separation because of the relative position of the valence and conduction band of SiC and those of PTF. The increase of ΔN reflects better electron transfer in the presence of SiC than in the presence of the PTF at the studied interface. The gel electrolyte used showed good stability, which is evident from the reproducible data observed at different times.

References

[1]   S. Steinberger, A. Mishra, E. Reinold, J. Levichkov, C. Uhrich, M. Pfeiffer, P. Bäuerle, Vacuum-processed small molecule solar cells based on terminal acceptor-substituted low-bandgap ligothiophenes, *Chemical Communications* **47** (2011) 1982-1984. https://doi.org/10.1039/C0CC04541A

[2]   T. Kono, D. Kumaki, J. Nishida, S. Tokito, Y. Yamashita, Dithienylbenzobis (thiadiazole) based organic semiconductors with low LUMO levels and narrow energy gaps, *Chemical Communications* **46** (2010) 3265-3267. https://doi.org/10.1039/B925151K

[3]   A. Mishra, C.-Q. Ma, P. Bäuerle, Functional Oligothiophenes: Molecular Design for Multidimensional Nanoarchitectures and Their Applications, *Chemical Reviews* **109(3)** (2009) 1141-1276. https://doi.org/10.1021/cr8004229

[4]   R. Tang, F. Zhang, Y. Fu, Q. Xu, X. Wang, X. Zhuang, D. Wu, A. Giannakopoulos, D. Beljonne, X. Feng, Efficient Approach to Electron-Deficient 1,2,7,8-Tetraazaperylene Derivatives, *Organic Letters* **16(18)** (2014) 4726-4729. https://doi.org/10.1021/ol502109y

[5]   T. Torroba, Poly-sulfur-nitrogen heterocycles via sulfur chlorides and nitrogen reagents, *Journal für praktische Chemie* **341(2)** (1999) 99-113. https://doi.org/10.1002/(SICI)1521-3897(199902)341:2%3C99::AID-PRAC99%3E3.0.CO;2-Z

[6]   M. Krompiec, S. Krompiec, H. Ignasiak, M. Łapkowski, P. Kuś, Ł. Stanek, R. Penczek, S. Lis, K. Staniński, M. Sajewicz, K. Gębarowska, Synthesis and electropolymerization of 3,5-dithienylpyridines, their complexes and N-methylpyridinium cations, *Synthetic Metals* **158(21–24)** (2008) 831-838. https://doi.org/10.1016/j.synthmet.2008.05.010

[7]   L. Akcelrud, Electroluminescent polymers, *Progress in Polymer Science* **28(6)** (2003) 875-962. https://doi.org/10.1016/S0079-6700(02)00140-5

[8]   H. Sirringhaus, N. Tessler, R.H. Friend, Integrated Optoelectronic Devices Based on Conjugated Polymers, *Science* **280** (1998) 1741-1744. https://doi.org/10.1126/science.280.5370.1741

[9]   P.R. Somani, S. Radhakrishnan, Electrochromic materials and devices: present and future, *Materials Chemistry and Physics* **77(1)** (2002) 117-133. https://doi.org/10.1016/S0254-0584(01)00575-2

[10]   D.T. McQuade, A.E. Pullen, T.M. Swager, Conjugated Polymer-Based Chemical Sensors, *Chemical Reviews* **100(7)** (2000) 2537-2574. https://doi.org/10.1021/cr9801014

[11]   J. Zhang, Y Hao, L Yang, H Mohammadi, N Vlachopoulos, L Sun, A Hagfeldt, E. Sheibani, Electrochemically polymerized poly (3, 4-phenylene-dioxythiophene) as efficient and transparent counter electrode for dye-sensitized solar cells, *Electrochimica Acta* **300** (2019) 482-488. https://doi.org/10.1016/j.electacta.2019.01.006

[12]   A. Malinauskas, Chemical deposition of conducting polymers, *Polymer* **42** (2001) 3957-3972. https://doi.org/10.1016/S0032-3861(00)00800-4

[13]   K. K. Kasem, M. Schiltz, S. H. Osman, Optical and Photoelectrochemical Investigation of Mixed Photoactive Poly 2,2',5,2'' ter-thiophene and Poly 2,2 bithiophene. Role of Intermixed Phases Created by the co-electro-polymerization process, *International Journal of Chemistry* **12(1)** (2020) 49. https://doi.org/10.5539/ijc.v12n1p49

[14]   S. H. Osman, A. Jeffers, K. K. Kasem, Electrochemical, Optical and Impedance Studies on Photoactive Assemblies Consists of Mixed TiO_2-CdS Particles Occluded in Poly 2,2' Bithiophene in Aqueous Acetate Electrolytes, *International Journal of Electrochemical Science* **14(12)** (2019) 10729-10744. https://doi.org/10.20964/2019.12.58

[15]   J. A. Joule, K. Mills, *Heterocyclic Chemistry*, Wiley- Blackwell Publishing Ltd, 2010. ISBN: 978-1-405-13300-5

[16]   H. Zhou, L. Yang, W. You, Rational design of high-performance conjugated polymers for organic solar cells, *Macromolecules* **45(2)** (2012) 607-632. https://doi.org/10.1021/ma201648t

[17]   B. Kan, M. Li, Q. Zhang, F. Liu, X. Wan, Y. Wang, W. Ni, G. Long, X. Yang, H. Feng, Y. Zuo, M. Zhang, F. Huang, Y. Cao, T. Russell, Y. Chen, A Series of Simple Oligomer-like Small Molecules Based on Oligothiophenes for Solution-Processed Solar Cells with High Efficiency, *Journal of the American Chemical Society* **137(11)** (2015) 3886-3893. https://doi.org/10.1021/jacs.5b00305

[18] B. Guo, X. Guo, W. Li, X. Meng, W. Ma, M. Zhang, Y. Li, A wide-band gap conjugated polymer for highly efficient inverted single and tandem polymer solar cells, *Journal of Materials Chemistry A* **4(34)** (2016) 13251-13258. https://doi.org/10.1039/C6TA04950H

[19] M. Suda, A New Photo-Control Method for Organic/Inorganic Interface Dipoles and Its Application to Photo-Controllable Molecular Devices, *Bulletin of the Chemical Society of Japan* **91** (2018) 19-28. https://doi.org/10.1246/bcsj.20170283

[20] M. O. Rodrigues, V. G. Isoppo, A. V. Moro, F. S. Rodembusch, Photoactive organic-inorganic hybrid materials: From silylated compounds to optical applications, *Journal of Photochemistry and Photobiology C: Photochemistry Reviews* **51** (2022) 100474. https://doi.org/10.1016/j.jphotochemrev.2021.100474

[21] K. K. Kasem, S. Menges, S. Jones, Photoelectrochemical studies on poly[1-(2-aminophenyl)pyrrole] - Creation of a photoactive inorganic–organic semiconductor interface (IOI), *Canadian Journal of Chemistry* **87(8)** (2009) 1109-1116. https://doi.org/10.1139/V09-079

[22] K. K. Kasem, H. Worley, M. Elmasry, Optical and Photoelectrochemical Studies on Photoactive Inorganic/Organic/Organic/ Interface Assemblies of CdS/poly 3-(2-thienyl) aniline/poly2,2 Bithiophene, *Advanced Composites and Hybrid Materials* **1** (2018) 748-758. https://doi.org/10.1007/s42114-018-0055-0

[23] B. N. Pushpakaran, A. S. Subburaj, S. B. Bayne, J. Mookken, Impact of silicon carbide semiconductor technology in Photovoltaic Energy System, *Renewable and Sustainable Energy Reviews* **55** (2016) 971-989. https://doi.org/10.1016/j.rser.2015.10.161

[24] Y. Zhang, Y. Zhang, X. Li, J. Dai, F. Song, X. Cao, X. Lyu, J. C. Crittenden, Enhanced Photocatalytic Activity of SiC-Based Ternary Graphene Materials: A DFT Study and the Photocatalytic Mechanism, *ACS Omega* 2019 **4(23)** (2019) 20142-20151. https://doi.org/10.1021/acsomega.9b01832

[25] K. K. Kasem, J. Pu, L. Cox, Photoactivities of Thiophene Monomer/Polymer Transition in Gel–Based Photoelectrochemical Assembly: A Theoretical/Experimental Approach, *International Journal of Electrochemical Science* **18(4)** (2023) 100077. https://doi.org/10.1016/j.ijoes.2023.100077

[26] J. H. Wu, S. C. Hao, Z. Lan, J. M. Lin, M. L. Huang, Y. F. Huang, L. Q. Fang, S. Yin, T. Sato, A Thermoplastic Gel Electrolyte for Stable Quasi-Solid-State Dye-Sensitized Solar Cells, *Advanced Functional Materials* **17(15)** (2007) 2645-2652. https://doi.org/10.1002/adfm.200600621

[27] F. Neese, Software update: The ORCA program system—Version 5.0, *WIREs Computational Molecular Science* **12(5)** (2022) e1606. https://doi.org/10.1002/wcms.1606

[28] G. Knizia, Intrinsic Atomic Orbitals: An Unbiased Bridge between Quantum Theory and Chemical Concepts, *Journal of Chemical Theory and Computation* **9(11)** (2013) 4834-4843. https://doi.org/10.1021/ct400687b

[29] J. Tauc, Optical properties and electronic structure of amorphous Ge and Si, *Materials Research Bulletin* **3(1)** (1968) 37-46. https://doi.org/10.1016/0025-5408(68)90023-8

[30] T. Koopmans, Über die Zuordnung von Wellenfunktionen und Eigenwerten zu den einzelnen Elektronen eines Atoms, *Physica* **1 (1–6)** (1934) 104-113. https://doi.org/10.1016/S0031-8914(34)90011-2

[31] M. Mobin, R. Aslam, J. Aslam, Synergistic effect of cationic gemini surfactants and butanol on the corrosion inhibition performance of mild steel in acid solution, *Materials Chemistry and Physics* **223** (2019) 623-633. https://doi.org/10.1016/j.matchemphys.2018.11.032

[32] C. Langpoklakpam, A. C. Liu, K. H. Chu, L. H. Hsu, W. C. Lee, S. C. Chen, C. W. Sun, M. H. Shih, K. Y. Lee, H. C. Kuo. Review of Silicon Carbide Processing for Power MOSFET, *Crystals* **12(1)** (2022) 245. https://doi.org/10.3390/cryst12020245

[33]   J. Jian, J. Sun, A Review of Recent Progress on Silicon Carbide for Photoelectro-chemical Water Splitting, *Solar RRL* **4(7)** (2020) 2000111. https://doi.org/10.1002/solr.202000111

[34]   P. Sharma, S.C. Katyal, Effect of Cd and Pb impurities on the optical properties of fresh evaporated amorphous (As$_2$Se$_3$)$_{90}$Ge$_{10}$ thin films, *Journal of Physics D: Applied Physics* **40(7)** (2007) 2115. https://doi.org/10.1088/0022-3727/40/7/038

[35]   T. C. Sabari Girisun, S. Dhanushkodi, Linear and nonlinear optical properties of tris thiourea zinc sulphate single crystals, *Crystal Research & Technology* **44(12)** (2009) 1297-1302. https://doi.org/10.1002/crat.200900351

[36]   H. Wei, H. Eilers, Electrical conductivity of thin-film composites containing silver nanoparticles embedded in a dielectric fluropolymer matrix, *Thin Solid Films* **517(2)** (2008) 575-581. https://doi.org/10.1016/j.tsf.2008.06.093

[37]   F. Spadavecchia, S. Ardizzone, G. Cappelletti, L. Falciola, M. Ceotto, D. Lotti, *Journal of Applied Electrochemistry* **43** (2013) 217-225. https://doi.org/10.1007/s10800-012-0485-2

[38]   E. Go, H. Jin, S. Yoon, S. Park, S.H. Park, H. Yu, H.J. Son, Unraveling the Origin of Dark Current in Organic Bulk Heterojunction Photodiodes for Achieving High Near-Infrared Detectivity, *ACS Photonics* **9(6)** (2022) 2056-2065. https://doi.org/10.1021/acsphotonics.2c00193

[39]   C. Li, Y. Bando, M. Liao, Y. Koide, D. Golberg, Visible-blind deep-ultraviolet Schottky photodetector with a photocurrent gain based on individual Zn$_2$GeO$_4$ nanowire, *Applied Physics Letters* **97** (2010) 161102. https://doi.org/10.1063/1.3491212

[40]   H. Kaiser K. D. Beccu, M. A. Gutjahr, Abschätzung der porenstruktur poröser elektroden aus impedanzmessungen, *Electrochimica Acta* **21** (1976) 539-543. https://doi.org/10.1016/0013-4686(76)85147-X

[41]   K.K. Kasem, M. Tom, M. Tahir, L. Cox, Electrochemical and optical studies on photoactive BiVO$_4$-TiO$_2$/poly 3,4-ethylenedioxythiophene assemblies in gel electrolyte: Role of inorganic/organic interfaces in surface functionalization, *Journal of Electrochemical Science and Engineering* **13(6)** (2023) 1037-1050. https://doi.org/10.5599/jese.1951